Dyes and Pigments 113 (2015) 390–401

Contents lists available at ScienceDirect

Dyes and Pigments

journal homepage: www.elsevier.com/locate/dyepig

The effect of the number, position, and shape of methoxy groups in triphenylamine donors on the performance of dye-sensitized solar cells

Se Hun Kim [a, 1, 2], Jun Choi [b, 1], Chun Sakong [a, 2], Jin Woong Namgoong [a, 2], Woosung Lee [c], Dong Hoe Kim [a, 2], Boeun Kim [d], Min Jae Ko [d], Jae Pil Kim [a, *, 2]

[a] Department of Materials Science and Engineering, Seoul National University, Seoul 151-744, Republic of Korea
[b] Material R&D Team 4, LG Display Co., Ltd., Paju-si, Gyeongki-do 413-779, Republic of Korea
[c] ICT Textile & Apparel R&BD Group, Korea Institute of Industrial Technology (KITECH), Ansan-si, Gyeonggi-do 426-910, Republic of Korea
[d] Solar Cell Research Center, Materials Science and Technology Division, Korea Institute of Science and Technology (KIST), Seoul 136-791, Republic of Korea

ARTICLE INFO

Article history:
Received 1 August 2014
Received in revised form
4 September 2014
Accepted 6 September 2014
Available online 16 September 2014

Keywords:
Dye-sensitized solar cell
Triphenylamine dye
Electron donor
Methoxy group
Bathochromic shift
Dihedral angle

ABSTRACT

Four new organic photosensitizers (**SH-11~14**) that introduced methoxy groups as an additional donor were synthesized, and used in dye-sensitized solar cells. The dyes were designed in order to investigate the effects on the dye photophysical properties and the cell photovoltaic performance, by the number, position, and shape of methoxy groups introduced at the *para-*/*ortho-* and *para-*/*meta-* and *para-*(open or closed ring shape) positions on the triphenylamine donor. The introduction of methoxy groups led to bathochromic shift of the absorption spectrum, and enhancement of the molar extinction coefficient of the dyes. Their introduction decreased the amount of dye adsorbed on TiO_2 surface, due to the increased steric hindrance. As their number increased, an open-circuit voltage value decreased. All things considered, the dye (**SH-14**) with closed ring shape shows the best conversion efficiency of 6.01% under AM 1.5G conditions (**N719** dye's 7.59% under the same conditions).

1. Introduction

Since Grätzel et al. reported Ru-based photosensitizers in 1991, dye-sensitized solar cells (DSSCs) have been considered as promising converters of solar energy, due to their low-cost fabrication, environmental friendliness, and high power conversion efficiency [1]. As one of the most important components in DSSCs, the photosensitizer plays a crucial role in achieving high DSSC efficiency. Thus, many photosensitizers, such as ruthenium complex dyes, metal-free organic dyes containing diverse molecular structures, and organometallic dyes that employ porphyrins or phthalocyanines, have been extensively studied by researchers around the world [2]. So far, Ru complex sensitizers (N3, **N719**, and black dye) and organic dyes containing triphenylamine (TPA) moiety have been reported to give high power conversion efficiencies of over 11% and 10% under AM 1.5G irradiation, respectively [3]. Recently, the highest efficiency of over 12% has been achieved from DSSCs co-sensitized by zinc porphyrin sensitizers (YD2-*o*-C8 and Y123) [4]. Porphyrin-based photosensitizer efficiencies have sharply improved in recent years, by the intense efforts of countless research scientists to achieve high efficiency [2c].

Although metal-free organic dye efficiencies are somewhat lower than those of Ru complex photosensitizers and zinc porphyrin photosensitizers, organic dyes as alternatives to metal complex photosensitizers are still promising candidates for the photosensitizers of DSSCs, due to their many advantages, such as relatively low cost, simple synthetic route, high molar extinction coefficient, diversity of molecular structure, and environmental friendliness. Until now, organic dyes of diverse structures containing carbazole [5], coumarin [6], fluorine [7], indoline [8], perylene [9], phenothiazine [10], phenoxazine [11], squaraine [12], tetrahydroquionoline [13], and triphenylamine [3d,14] have been extensively studied. Among them, triphenylamine-based and quinoxaline-based organic dyes showed higher efficiency compared to those of different structures [3d,3e].

TPA-based organic dyes are still under intense academic investigation, due to their prominent electron donation and hole-

---

* Corresponding author. Tel.: +82 2 880 7187; fax: +82 2 880 7238.
E-mail address: jaepil@snu.ac.kr (J.P. Kim).
[1] Both authors contributed equally to the research.
[2] Tel.: +82 2 880 7187; fax: +82 2 885 1748.

http://dx.doi.org/10.1016/j.dyepig.2014.09.014
0143-7208/© 2014 Elsevier Ltd. All rights reserved.

transport ability [15,2d]. To improve DSSC efficiency, photosensitizers are required to have bathochromic shifts, broad absorption spectra, and/or enhancement of molar extinction coefficients. To attain this end in most organic dyes (D—π—A structure) having push—pull structure, two strategies were adopted: extending the π-conjugation length of molecule (D—π—π—A structure), and introducing an additional donor (AD) to the main donor (D) (AD—D—π—A or D—D—π—A structure). However, organic dyes having D—π—π—A structure can have close π—π aggregation, which can lead to self-quenching, and reduction of electron injection into TiO_2 [16]. Compared to D—π—π—A structure, organic dyes with AD—D—π—A structure benefit from the lower possibility of close π—π aggregation. They can also have the advantages of bathochromic shift of the absorption spectrum, and enhancement of the molar extinction coefficient [17]. Therefore, organic dyes with AD—D—π—A structure have recently been studied by several groups [17,18]. The aforementioned researches were oriented to the effects of the introduction of sterically bulky moieties, such as carbazole, diphenylamine group, alkoxy substituted phenyl group, and heterocyclic ring, as additional donors at the *para*-position of the TPA donor part. However, their introduction to the TPA donor part decreased the amount of dye adsorbed on TiO_2 surface, due to the increased steric hindrance.

Therefore, to minimize this drawback, we designed and synthesized four new TPA-based organic dyes (**D1** [19] that has been previously published, **SH-11~14** as shown in Fig. 1). The dyes have AD—D—π—A structure, which has the TPA moiety as a main electron donor (D), methoxy groups as an additional electron donor (AD), furan moiety as a π-bridge (π), and a cyanoacrylic acid group as an electron acceptor (A). The methoxy groups as an additional donor can lead not only to bathochromic shift of the absorption spectrum and enhancement of the molar extinction coefficient, but also to relatively smaller steric hindrance, compared to the sterically bulky moieties. The effects of the number, position, and shape of the methoxy groups attached to the TPA donor part were investigated by the dye photophysical and electrochemical properties, and the cells photovoltaic performance. To the best of our knowledge, this is the first report studying the effects of the introduction of an additional donor of various number, position, and shape to the TPA donor moiety for efficiency improvement. To gain further insight into their effects, density functional theory (DFT) calculations of all the dyes were carried out, using the B3LYP/6-31G(d,p) level. Electrochemical impedance spectroscopy (EIS) was used to study their interfacial charge transfer. The synthetic routes of the new dyes are depicted in Scheme 1.

2. Experimental section

2.1. Materials and regents

All reactions were performed under nitrogen atmosphere. 3,4-Dimethoxyaniline, 6-amino-1,4-benzodioxane, 2,4-dimethoxyiodobenzene, and 4-bromoaniline from TCI and 4-iodoanisole, KI, CuI, 1,10-phenanthroline, tetrakis(triphenylphosphine)palladium(0), 5-formyl-2-furan-boronic acid, cyanoacetic acid, and piperidine from Sigma—Aldrich were purchased and used as received without further purification. All solvents (toluene anhydrous, tetrahydrofuran anhydrous, and acetonitrile anhydrous) were obtained from Sigma—Aldrich and used as received. Other chemicals were reagent grade and used without further purification.

2.2. Analytical instruments and measurements

^1H NMR and ^{13}C NMR spectra were recorded on a Bruker Avance 300 and 500 MHz (Seoul National University National Center for inter-University Research Facilities) with the chemical shifts against TMS. Mass spectra were measured with a JEOL JMS-600W mass spectrometer (Seoul National University National Center for inter-University Research Facilities). Elemental analyses were carried out with a Flash EA 1112 elemental (C,N,S) analyzer. UV—vis spectra and photoluminescence spectra were recorded on a Hewlett—Packard 8452A spectrophotometer and Shimadzu RF-5301PC spectrofluorometer, respectively. Cyclic voltammetry spectra were obtained using a three-electrode cell with a 273A (Princeton applied research, Inc.). The measurement was carried out using an Ag wire (Ag/Ag^+), a glassy carbon and a platinum wire as a reference, a working and a counter electrode, respectively, in CH_2Cl_2 solution containing 0.1 M tetrabutylammonium tetrafluoroborate as a supporting electrolyte. A standard ferrocene/ferrocenium (Fc/Fc^+) redox couple was used to calibrate the oxidation peak. Photocurrent—voltage (*I*—*V*) measurements were performed using a Keithley model 2400 source measure unit. Incident photon-to-current conversion efficiency (IPCE) was measured as a function of wavelength from 300 nm to 1000 nm using a specially designed IPCE system for the dye-sensitized solar cell (PV measurements, Inc.).

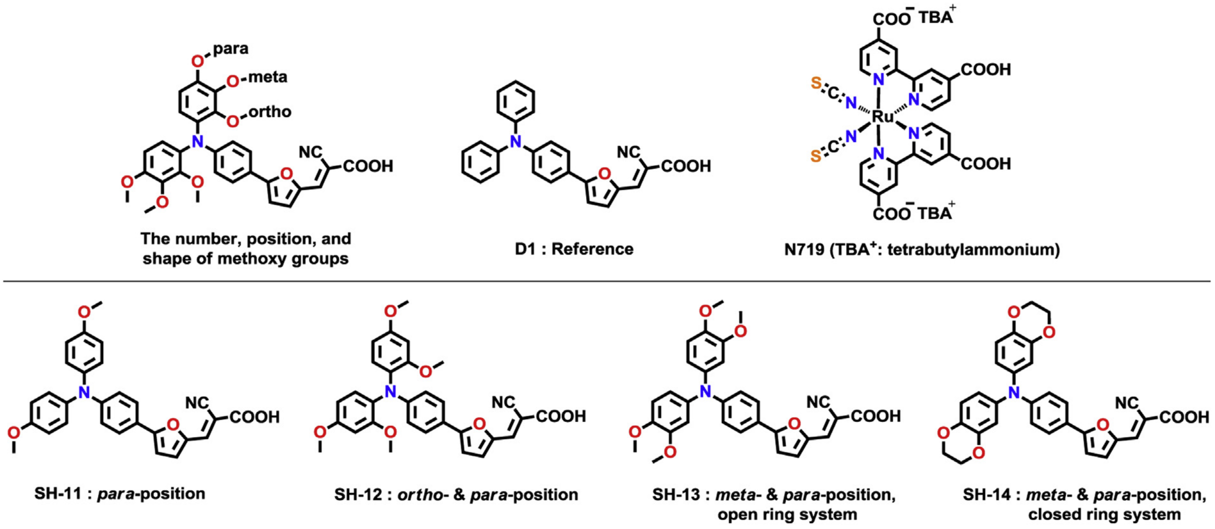

Fig. 1. Molecular structures of **D1**, **N719**, **SH-11**, **SH-12**, **SH-13**, and **SH-14**.

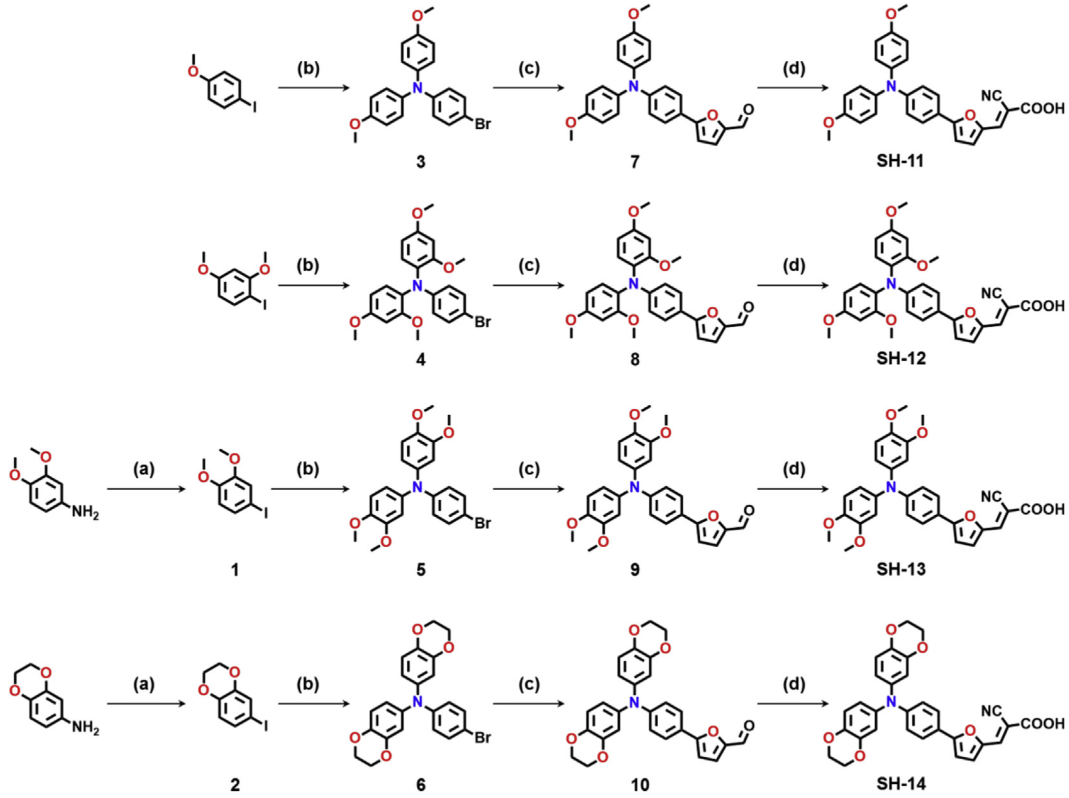

Scheme 1. Synthesis of **SH-11**, **SH-12**, **SH-13**, and **SH-14**: (a) i) HCl, $NaNO_2$, H_2O ii) KI, H_2O (b) 4-bromoaniline, CuI, 1,10-phenanthroline, KOH, toluene (c) 5-formyl-2-furan-boronic acid, $Pd(PPh_3)_4$, K_2CO_3, THF (d) cyanoacetic acid, piperidine, acetonitrile.

2.3. Fabrication of dye-sensitized solar cells and photovoltaic measurements

The nanocrystalline TiO_2 working electrode comprised a TiO_2 transparent layer (20 nm, synthesized) and a TiO_2 scattering layer (250 nm, G1). The Pt-coated counter electrode was prepared by a reported procedure [20]. TiO_2 electrodes were immersed in *tert*-butanol–acetonitrile (1:1) solution containing the dyes at 0.5 mM for 40 h at ambient temperature. They were then washed with ethanol and dried under a stream of nitrogen. The working and counter electrodes were sealed with Surlyn (60 μm, Dupont) and the electrolyte was injected through a hole in the counter electrode. The electrolyte comprised 0.7 M 1-methyl-3-propylimidazolium iodide (PMII), 0.2 M LiI (Aldrich), 0.05 M I_2 (Aldrich), and 0.5 M 4-*tert*-butylpyridine (TBP, Aldrich) in a mixed solvent of acetonitrile and valeronitrile (v/v, 85/18). The active area of the dye-coated TiO_2 film was 0.269–0.284 cm^2 working area, measured by analyzing images from a CCD camera (moticam 1000). TiO_2 film thickness was measured by an α-step surface profiler (KLA tencor). Photocurrent–voltage (I–V) measurements were performed using a Keithley model 2400 source meter. A class-A solar simulator (Newport) equipped with 150 W Xe lamp was used as a light source. Light intensity was adjusted with an NREL-calibrated Si solar cell with KG-5 filter for approximating 1 sunlight intensity. Photocurrent–voltage measurement of the dye-sensitized solar cells was performed with an aperture mask. Incident photon-to-current conversion efficiency (IPCE) was measured as a function of wavelength from 300 to 1000 nm using a specially designed IPCE system for dye-sensitized solar cells (PV measurements, Inc.). A 75 W xenon lamp was used as a light source for generating monochromatic beams. Calibration was performed using a silicon photodiode, which was calibrated using a NIST-calibrated photodiode G425 standard. IPCE values were measured under halogen bias light at a low chopping speed of 10 Hz.

2.4. Synthesis of dyes

2.4.1. 4-Iodo-1,2-dimethoxybenzene (**1**)

A mechanically stirred mixture of **3,4-dimethoxyaniline** (5.36 g, 35 mmol) and 36% HCl (50 mL) was cooled to −5 °C. A solution of $NaNO_2$ (2.90 g, 42 mmol) in 20 mL H_2O was cooled to 0 °C and slowly added while maintaining the temperature at −5 °C. The final solution was stirred at 0 °C for 30 min. A solution of KI (11.62 g, 70 mmol) in 30 mL H_2O was added dropwise keeping the temperature between 0 and 5 °C. The resulting mixture was stirred overnight and extracted twice with diethyl ether. The organic layer was consecutively washed with a concentrated $NaHSO_3$ solution, 5% NaOH and water and dried over $MgSO_4$. The solvent was removed under reduced pressure and the crude product was purified by column chromatography using silica gel and dichloromethane–hexane (3:1; v/v) as the eluent to give **1**, a pale yellow oil phase (6.91 g, 74.78%). ^1H NMR (500 MHz, d_6-DMSO, ppm): δ 7.23 (d, $J = 8.38$ Hz, 1H), 7.19 (s, 1H), 6.78 (d, $J = 8.39$ Hz, 1H), 3.75 (s, $-OCH_3$, 3H), 3.73 (s, $-OCH_3$, 3H).

2.4.2. 6-Iodo-1,4-benzodioxane (**2**)

A mechanically stirred mixture of **6-amino-1,4-benzodioxane** (5.29 g, 35 mmol) and 36% HCl (50 mL) was cooled to −5 °C. A solution of $NaNO_2$ (2.90 g, 42 mmol) in 20 mL H_2O was cooled to 0 °C and slowly added while maintaining the temperature at −5 °C. The final solution was stirred at 0 °C for 30 min. A solution of KI (11.62 g, 70 mmol) in 30 mL H_2O was added dropwise keeping the temperature between 0 and 5 °C. The resulting mixture was stirred overnight and extracted twice with diethyl ether. The organic layer was consecutively washed with a concentrated $NaHSO_3$ solution, 5% NaOH and water and dried over $MgSO_4$. The solvent was removed under reduced pressure and the crude product was purified by column chromatography using silica gel and dichloromethane–hexane (3:2; v/v) as the eluent to give **2**, a pale yellow oil phase (8.64 g, 94.22%). ^1H NMR (500 MHz, d_6-DMSO, ppm): δ 7.18 (s, 1H), 7.13 (d, $J = 8.45$ Hz, 1H), 6.68 (d, $J = 8.45$ Hz, 1H), 4.22 (s, $-OCH_2CH_2O-$, 4H).

2.4.3. 4-Bromo-N,N-bis(4-methoxyphenyl)aniline (*3*)

To a stirred solution of **4-iodoanisole** (5.85 g, 25 mmol), 4-bromoaniline (1.72 g, 10 mmol), and 1,10-phenanthroline (0.18 g, 1 mmol) in toluene (100 mL) were added potassium hydroxide (5.61 g, 100 mmol) and copper(I) iodide (0.19 g, 1 mmol). The reaction mixture was heated under reflux for 24 h at 125 °C. The crude product was extracted into dichloromethane, and the organic layer was washed with 1 N HCl solution, brine, and water. The organic layer was dried with anhydrous $MgSO_4$ and then the solvent was removed in vacuo. The residue was purified by column chromatography using silica gel and dichloromethane–hexane (1:1; v/v) as the eluent to give **3** (2.39 g, 62.2%). ^1H NMR (500 MHz, d_6-DMSO, ppm): δ 7.31 (d, $J = 9.0$ Hz, 2H), 7.04–7.02 (m, 4H), 6.93–6.91 (m, 4H), 6.67 (d, $J = 9.0$ Hz, 2H), 3.74 (s, $-OCH_3 \times 2$, 6H). ^{13}C NMR (126 MHz, $CDCl_3$, ppm): δ 156.0, 147.9, 140.6, 131.7, 127.7, 126.5, 121.9, 114.8, 114.2, 112.4, 55.5. HRMS (*m*/*z*): calcd. for ($C_{20}H_{18}BrNO_2$): 383.0520, found: 383.0516 [EI+]. Anal. Cald for ($C_{20}H_{18}BrNO_2$): C, 62.51; H, 4.72; N, 3.65. Found: C, 62.39; H, 4.70; N, 3.52.

2.4.4. N-(4-Bromophenyl)-N-(2,4-dimethoxyphenyl)-2,4-dimethoxyaniline (*4*)

Product 4 was synthesized according to the procedure as described above for synthesis of **3**. To a stirred solution of **2,4-dimethoxyiodobenzene** (6.60 g, 25 mmol), 4-bromoaniline (1.72 g, 10 mmol), and 1,10-phenanthroline (0.18 g, 1 mmol) in toluene (100 mL) were added potassium hydroxide (5.61 g, 100 mmol) and copper(I) iodide (0.19 g, 1 mmol). Eluent: dichloromethane–hexane (2:1; v/v), **product 4** (2.97 g, 67.0%). ^1H NMR (300 MHz, $CDCl_3$, ppm): δ 7.13–7.06 (m, 4H), 6.45–6.36 (m, 4H), 6.27 (s, 2H), 3.73 (s, $-OCH_3 \times 2$, 6H), 3.65 (s, $-OCH_3 \times 2$, 6H). ^{13}C NMR (126 MHz, $CDCl_3$, ppm): δ 158.9, 156.8, 148.3, 131.1, 130.3, 127.8, 116.1, 109.2, 104.9, 100.1, 55.7, 55.5. HRMS (*m*/*z*): calcd. for ($C_{22}H_{22}BrNO_4$): 443.0732, found: 443.0731 [EI+]. Anal. Cald for ($C_{22}H_{22}BrNO_4$): C, 59.47; H, 4.99; N, 3.15. Found: C, 60.06; H, 4.98; N, 2.98.

2.4.5. N-(4-Bromophenyl)-N-(3,4-dimethoxyphenyl)-3,4-dimethoxyaniline (*5*)

Product 5 was synthesized according to the procedure as described above for synthesis of **3**. To a stirred solution of **1** (6.60 g, 25 mmol), 4-bromoaniline (1.72 g, 10 mmol), and 1,10-phenanthroline (0.18 g, 1 mmol) in toluene (100 mL) were added potassium hydroxide (5.61 g, 100 mmol) and copper(I) iodide (0.19 g, 1 mmol). Eluent: dichloromethane–hexane (3:1; v/v), **product 5** (2.84 g, 64.1%). ^1H NMR (500 MHz, d_6-DMSO, ppm): δ 7.32 (d, $J = 8.9$ Hz, 2H), 6.93 (d, $J = 8.6$ Hz, 2H), 6.73–6.70 (m, 4H), 6.63 (d, $J = 8.5$ Hz, 2H), 3.74 (s, $-OCH_3 \times 2$, 6H), 3.64 (s, $-OCH_3 \times 2$, 6H). ^{13}C NMR (126 MHz, $CDCl_3$, ppm): δ 149.6, 147.7, 145.7, 140.8, 131.8, 122.6, 117.3, 112.9, 111.9, 109.3, 56.1, 55.9. HRMS (*m*/*z*): calcd. for ($C_{22}H_{22}BrNO_4$): 443.0732, found: 443.0736 [EI+]. Anal. Cald for ($C_{22}H_{22}BrNO_4$): C, 59.47; H, 4.99; N, 3.15. Found: C, 59.67; H, 4.89; N, 3.17.

2.4.6. N-(4-Bromophenyl)-N-(2,3-dihydrobenzo[b][1,4]dioxin-6-yl)-2,3-dihydrobenzo[b][1,4]dioxin-6-amine (*6*)

Product 6 was synthesized according to the procedure as described above for synthesis of **3**. To a stirred solution of **2** (6.55 g, 25 mmol), 4-bromoaniline (1.72 g, 10 mmol), and 1,10-phenanthroline (0.18 g, 1 mmol) in toluene (100 mL) were added potassium hydroxide (5.61 g, 100 mmol) and copper(I) iodide (0.19 g, 1 mmol). Eluent: dichloromethane–hexane (1:1; v/v), **product 6** (2.67 g, 60.6%). ^1H NMR (500 MHz, d_6-DMSO, ppm): δ 7.33 (d, $J = 8.56$ Hz, 2H), 6.83 (d, $J = 8.44$ Hz, 2H), 6.71 (d, $J = 8.56$ Hz, 2H), 6.55–6.53 (m, 4H), 4.22 (s, $-OCH_2CH_2O- \times 2$, 8H). ^{13}C NMR (126 MHz, $CDCl_3$, ppm): δ 147.5, 143.9, 141.1, 140.1, 131.8, 122.9, 118.4, 117.7, 114.1, 112.9, 64.4, 64.3. HRMS (*m*/*z*): calcd. for ($C_{22}H_{18}BrNO_4$): 439.0419, found: 439.0420 [EI+]. Anal. Cald for ($C_{22}H_{18}BrNO_4$): C, 60.01; H, 4.12; N, 3.18. Found: C, 59.95; H, 4.23; N, 3.11.

2.4.7. 5-(4-(Bis(4-methoxyphenyl)amino)phenyl)furan-2-carbaldehyde (*7*)

Under N_2 atmosphere, a mixture of **3** (2.31 g, 6 mmol), 5-formyl-2-furan-boronic acid (0.92 g, 6.6 mmol), $Pd(PPh_3)_4$ (0.35 g, 0.3 mmol), 2 M aqueous solution of K_2CO_3 (7.49 mL) in dry THF (50 mL) was heated under reflux for overnight. The reaction mixture extracted with CH_2Cl_2, water and brine. The organic layer was dried with anhydrous $MgSO_4$ and then the solvent was removed in vacuo. The residue was purified by column chromatography using silica gel and dichloromethane–methanol (50:1; v/v) as the eluent to give **7** (0.94 g, 39.2%). ^1H NMR (500 MHz, d_6-DMSO, ppm): δ 9.51 (s, $-CHO$, 1H), 7.66 (d, $J = 8.86$ Hz, 2H), 7.61 (d, $J = 3.77$ Hz, 2H), 7.12–7.10 (m, 4H), 6.97 (d, $J = 8.91$ Hz, 4H), 6.78 (d, $J = 8.88$ Hz, 2H), 3.76 (s, $-OCH_3 \times 2$, 6H). ^{13}C NMR (126 MHz, $CDCl_3$, ppm): δ 176.6, 160.3, 156.6, 151.4, 150.2, 139.9, 127.3, 126.4, 120.2, 119.0, 114.9, 105.8, 55.5. HRMS (*m*/*z*): calcd. for ($C_{25}H_{21}NO_4$): 399.1470, found: 399.1469 [EI+]. Anal. Cald for ($C_{25}H_{21}NO_4$): C, 75.17; H, 5.30; N, 3.51. Found: C, 75.05; H, 5.33; N, 3.58.

2.4.8. 5-(4-(Bis(2,4-dimethoxyphenyl)amino)phenyl)furan-2-carbaldehyde (*8*)

Product 8 was synthesized according to the procedure as described above for synthesis of **7**. A mixture of **4** (2.66 g, 6 mmol), 5-formyl-2-furan-boronic acid (0.92 g, 6.6 mmol), $Pd(PPh_3)_4$ (0.35 g, 0.3 mmol), 2 M aqueous solution of K_2CO_3 (7.49 mL) in dry THF (50 mL) was heated under reflux for overnight. Eluent: dichloromethane–methanol (50:1; v/v), **product 8** (0.91 g, 33.0%). ^1H NMR (500 MHz, $CDCl_3$, ppm): δ 9.51 (s, $-CHO$, 1H), 7.68 (d, $J = 8.75$ Hz, 2H), 7.55 (d, $J = 8.95$ Hz, 2H), 7.47 (d, $J = 3.73$ Hz, 1H), 6.58 (d, $J = 3.75$ Hz, 1H), 6.54 (s, 2H), 6.49–6.46 (m, 4H), 3.82 (s, $-OCH_3 \times 2$, 6H), 3.74 (s, $-OCH_3 \times 2$, 6H). ^{13}C NMR (126 MHz, $CDCl_3$, ppm): δ 176.6, 160.2, 149.9, 149.7, 146.2, 140.8, 140.1, 132.1, 132.0, 131.9, 131.8, 130.9, 126.3, 120.6, 119.7, 118.0, 117.3, 112.2, 111.9, 109.8, 109.3, 106.0, 56.1, 56.0. HRMS (*m*/*z*): calcd. for ($C_{27}H_{25}NO_6$): 459.1682, found: 459.1684 [FAB+]. Anal. Cald for ($C_{27}H_{25}NO_6$): C, 70.58; H, 5.48; N, 3.05. Found: C, 70.48; H, 5.52; N, 3.00.

2.4.9. 5-(4-(Bis(3,4-dimethoxyphenyl)amino)phenyl)furan-2-carbaldehyde (*9*)

Product 9 was synthesized according to the procedure as described above for synthesis of **7**. A mixture of **5** (2.66 g, 6 mmol), 5-formyl-2-furan-boronic acid (0.92 g, 6.6 mmol), $Pd(PPh_3)_4$ (0.35 g, 0.3 mmol), 2 M aqueous solution of K_2CO_3 (7.49 mL) in dry THF (50 mL) was heated under reflux for overnight. Eluent: dichloromethane–methanol (100:1; v/v), **product 9** (0.87 g, 31.6%). ^1H NMR (500 MHz, d_6-DMSO, ppm): δ 9.50 (s, $-CHO$, 1H), 7.67 (d, $J = 8.81$ Hz, 2H), 7.61 (d, $J = 3.72$ Hz, 2H), 6.97 (d, $J = 8.60$ Hz, 2H), 6.83–6.80 (m, 4H), 6.73 (d, $J = 8.53$ Hz, 2H), 3.76 (s, $-OCH_3 \times 2$, 6H), 3.67 (s, $-OCH_3 \times 2$, 6H). ^{13}C NMR (126 MHz, $CDCl_3$, ppm): δ 176.6, 160.2, 151.5, 149.9, 149.7, 146.2, 140.8, 140.1, 132.1, 132.0, 131.9, 131.8, 128.6, 128.4, 126.3, 122.6, 119.7, 118.0, 112.2, 111.9, 109.8, 106.0, 56.1, 56.0. HRMS (*m*/*z*): calcd. for ($C_{27}H_{25}NO_6$): 459.1682, found:

459.1688 [EI+]. Anal. Cald for ($C_{27}H_{25}NO_6$): C, 70.58; H, 5.48; N, 3.05. Found: C, 70.40; H, 5.47; N, 3.08.

2.4.10. 5-(4-(Bis(2,3-dihydrobenzo[b][1,4]dioxin-6-yl)amino)phenyl)furan-2-carbaldehyde (**10**)

Product 10 was synthesized according to the procedure as described above for synthesis of **7**. A mixture of **6** (2.64 g, 6 mmol), 5-formyl-2-furan-boronic acid (0.92 g, 6.6 mmol), $Pd(PPh_3)_4$ (0.35 g, 0.3 mmol), 2 M aqueous solution of K_2CO_3 (7.49 mL) in dry THF (50 mL) was heated under reflux for overnight. Eluent: dichloromethane–methanol (50:1; v/v), **product 10** (1.18 g, 43.3%). ^{1}H NMR (500 MHz, d_6-DMSO, ppm): δ 9.51 (s, –CHO, 1H), 7.67 (d, $J = 8.74$ Hz, 2H), 7.61 (d, $J = 3.92$ Hz, 1H), 7.04 (d, $J = 3.73$ Hz, 1H), 6.88 (d, $J = 7.37$ Hz, 2H), 6.82 (d, $J = 8.76$ Hz, 2H), 6.65–6.63 (m, 4H), 4.24 (s, $-OCH_2CH_2O- \times 2$, 8H). ^{13}C NMR (126 MHz, $CDCl_3$, ppm): δ 176.6, 160.3, 151.5, 149.7, 144.0, 140.7, 140.4, 126.3, 120.6, 119.8, 119.2, 117.8, 114.9, 105.9, 64.4, 64.3. HRMS (*m*/*z*): calcd. for ($C_{27}H_{21}NO_6$): 455.1369, found: 455.1372 [EI+]. Anal. Cald for ($C_{27}H_{21}NO_6$): C, 71.20; H, 4.65; N, 3.08. Found: C, 71.18; H, 4.68; N, 3.11.

2.4.11. (E)-3-(5-(4-(Bis(4-methoxyphenyl)amino)phenyl)furan-2-yl)-2-cyanoacrylic acid (**SH-11**)

Carbaldehyde 7 (200 mg, 0.5 mmol), cyanoacetic acid (0.13 g, 1.5 mmol) and piperidine (0.20 mL, 2 mmol) were added to anhydrous CH_3CN. After the mixture was heated under reflux for 8 h, the solution was extracted with CH_2Cl_2 and 0.1 M HCl aqueous solution. The organic phase was dried over anhydrous $MgSO_4$ and the solvent was removed in vacuo. The crude product was purified by column chromatography using silica gel and dichloromethane–methanol (5:1; v/v) as the eluent to give a red solid **SH-11** (175 mg, 75.0%). ^{1}H NMR (500 MHz, d_6-DMSO, ppm): δ 7.98 (s, 1H), 7.71 (d, $J = 8.83$ Hz, 2H), 7.51 (d, $J = 3.75$ Hz, 1H), 7.14–7.12 (m, 5H), 6.97 (d, $J = 8.88$ Hz, 4H), 6.77 (d, $J = 8.85$ Hz, 2H), 3.76 (s, $-OCH_3 \times 2$, 6H). ^{13}C NMR (126 MHz, $CDCl_3$, ppm): δ 168.4, 162.0, 156.8, 150.7, 146.9, 139.5, 138.3, 127.5, 126.8, 119.4, 118.7, 116.1, 114.9, 107.8, 93.3, 55.5. HRMS (*m*/*z*): Calcd. for ($C_{28}H_{22}N_2O_5$): 466.1529, found: 466.1527 [FAB+]. Anal. Cald for ($C_{28}H_{22}N_2O_5$): C, 72.09; H, 4.75; N, 6.01. Found: C, 72.01; H, 4.88; N, 5.97.

2.4.12. 3-(5-(4-(Bis(2,4-dimethoxyphenyl)amino)phenyl)furan-2-yl)-2-cyanoacrylic acid (**SH-12**)

Product SH-12 was synthesized according to the procedure as described above for synthesis of **SH-11**. **Carbaldehyde 8** (230 mg, 0.5 mmol), cyanoacetic acid (0.13 g, 1.5 mmol) and piperidine (0.20 mL, 2 mmol) were added to anhydrous CH_3CN. Eluent: dichloromethane–methanol (6:1; v/v), a red solid **SH-12** (205 mg, 77.9%). ^{1}H NMR (500 MHz, d_6-DMSO, ppm): δ 7.63 (s, 1H), 7.53 (d, $J = 8.73$ Hz, 2H), 7.19 (d, $J = 8.61$ Hz, 2H), 7.10 (d, $J = 3.42$ Hz, 1H), 6.83 (d, $J = 3.44$ Hz, 1H), 6.69 (s, 2H), 6.55 (d, $J = 8.61$ Hz, 2H), 6.28 (d, $J = 8.70$ Hz, 2H), 3.78 (s, $-OCH_3 \times 2$, 6H), 3.65 (s, $-OCH_3 \times 2$, 6H). ^{13}C NMR (126 MHz, d_6-DMSO, ppm): δ 163.7, 160.0, 158.6, 155.9, 149.9, 145.8, 136.4, 133.6, 129.7, 127.0, 125.6, 125.4, 116.5, 116.3, 112.7, 106.7, 105.2, 99.3, 93.8, 55.1, 54.8. HRMS (*m*/*z*): Calcd. for ($C_{30}H_{26}N_2O_7$): 526.1740, found: 526.1743 [FAB+]. Anal. Cald for ($C_{30}H_{26}N_2O_7$): C, 68.43; H, 4.98; N, 5.32. Found: C, 68.35; H, 4.93; N, 5.29.

2.4.13. 3-(5-(4-(Bis(3,4-dimethoxyphenyl)amino)phenyl)furan-2-yl)-2-cyanoacrylic acid (**SH-13**)

Product SH-13 was synthesized according to the procedure as described above for synthesis of **SH-11**. **Carbaldehyde 9** (230 mg, 0.5 mmol), cyanoacetic acid (0.13 g, 1.5 mmol) and piperidine (0.20 mL, 2 mmol) were added to anhydrous CH_3CN. Eluent: dichloromethane–methanol (6:1; v/v), a red solid **SH-13** (190 mg, 72.2%). ^{1}H NMR (500 MHz, d_6-DMSO, ppm): δ 7.97 (s, 1H), 7.72 (d, $J = 8.90$ Hz, 2H), 7.51 (d, $J = 3.75$ Hz, 1H), 7.13 (d, $J = 3.80$ Hz, 1H), 6.98 (d, $J = 8.65$ Hz, 2H), 6.83 (s, 2H), 6.79 (d, $J = 8.90$ Hz, 2H), 6.75 (d, $J = 8.55$ Hz, 2H), 3.76 (s, $-OCH_3 \times 2$, 6H), 3.68 (s, $-OCH_3 \times 2$, 6H). ^{13}C NMR (126 MHz, $CDCl_3$, ppm): δ 167.8, 161.4, 150.2, 149.7, 147.1, 146.3, 139.8, 138.1, 126.6, 119.9, 119.5, 118.2, 116.2, 111.9, 109.9, 107.7, 94.3, 56.1, 56.0. HRMS (*m*/*z*): Calcd. for ($C_{30}H_{26}N_2O_7$): 526.1740, found: 526.1744 [FAB+]. Anal. Cald for ($C_{30}H_{26}N_2O_7$): C, 68.43; H, 4.98; N, 5.32. Found: C, 68.37; H, 4.94; N, 5.26.

2.4.14. 3-(5-(4-(Bis(2,3-dihydrobenzo[b][1,4]dioxin-6-yl)amino)phenyl)furan-2-yl)-2-cyanoacrylic acid (**SH-14**)

Product SH-14 was synthesized according to the procedure as described above for synthesis of **SH-11**. **Carbaldehyde 10** (0.228 mg, 0.5 mmol), cyanoacetic acid (0.13 mg, 1.5 mmol) and piperidine (0.20 mL, 2 mmol) were added to anhydrous CH_3CN. Eluent: dichloromethane–methanol (5:1; v/v), a red solid **SH-14** (203 mg, 77.7%). ^{1}H NMR (500 MHz, d_6-DMSO, ppm): δ 7.98 (s, 1H), 7.72 (d, $J = 8.82$ Hz, 2H), 7.51 (d, $J = 3.73$ Hz, 1H), 7.13 (d, $J = 3.74$ Hz, 1H), 6.88–6.6 (m, 2H), 6.79 (d, $J = 8.84$ Hz, 2H), 6.66–6.64 (m, 4H), 4.24 (s, $-OCH_2CH_2O- \times 2$, 8H). ^{13}C NMR (126 MHz, $CDCl_3$, ppm): δ 167.5, 161.9, 150.3, 147.0, 144.1, 140.9, 140.0, 126.7, 119.7, 119.4, 117.9, 116.0, 115.2, 107.8, 93.3, 64.4, 64.3. HRMS (*m*/*z*): Calcd. for ($C_{30}H_{22}N_2O_7$): 522.1427, found: 522.1423 [FAB+]. Anal. Cald for ($C_{30}H_{22}N_2O_7$): C, 68.96; H, 4.24; N, 5.36. Found: C, 68.83; H, 4.19; N, 5.31.

3. Results and discussion

3.1. Synthesis

The synthetic routes and structures of the dyes with methoxy groups are shown in Scheme 1 and Fig. 1. Synthesis of the dyes first involved a Sandmeyer reaction of 3,4-dimethoxyaniline and 6-amino-1,4-benzodioxane, which produced iodinated intermediates (**1** and **2**) for an Ullmann reaction [21]. Compounds **3**~**6** were derived from C–N coupling of the 4-iodoanisole, 2,4-dimethoxyiodobenzene, **1**, and **2** with 4-bromoaniline by the Ullmann reaction, respectively. Compounds **7**~**10** were subsequently produced by Suzuki couplings between compounds **3**~**6** and 5-formyl-2-furan-boronic acid, respectively. Finally, the organic dyes (**SH-11**~**14**) were synthesized, by Knoevenagel condensation reactions of the aldehydes (**7**~**10**) with cyanoacetic acid, in the presence of piperidine and acetonitrile. The first intermediates (**1** and **2**), which are simple structures, were identified by ^{1}H NMR. The remainder of the intermediates and organic dyes were confirmed by ^{1}H NMR, ^{13}C NMR, HRMS, and elemental analysis. **D1** (reference dye) was synthesized, according to the published method [19].

3.2. Photophysical properties of the dyes in solution and on TiO_2 film

The absorption spectra of the synthesized dyes in CH_2Cl_2 solution and on TiO_2 films are shown in Fig. 2(a) and (b), respectively. The dyes' absorption, emission and electrochemical properties are listed in Table 1. The absorption spectra show two major bands, below *ca.* 400 nm, and at *ca.* 400–600 nm. The absorption in the UV region was attributed to localized π–π^* transitions; the band in the visible region was ascribed to intra-molecular charge transfer (ICT) from the TPA-based donor part to the acceptor [23].

The absorption maxima (λ_{max}) of **SH-11**~**14** with methoxy groups on the TPA donor are at 504, 504, 504, and 502 nm, respectively. The introduction of additional methoxy groups at *para*-(**SH-11**), *ortho*- and *para*-(**SH-12**), or *meta*- and *para*-(**SH-13**~**14**) positions on the TPA donor increased the electron donating

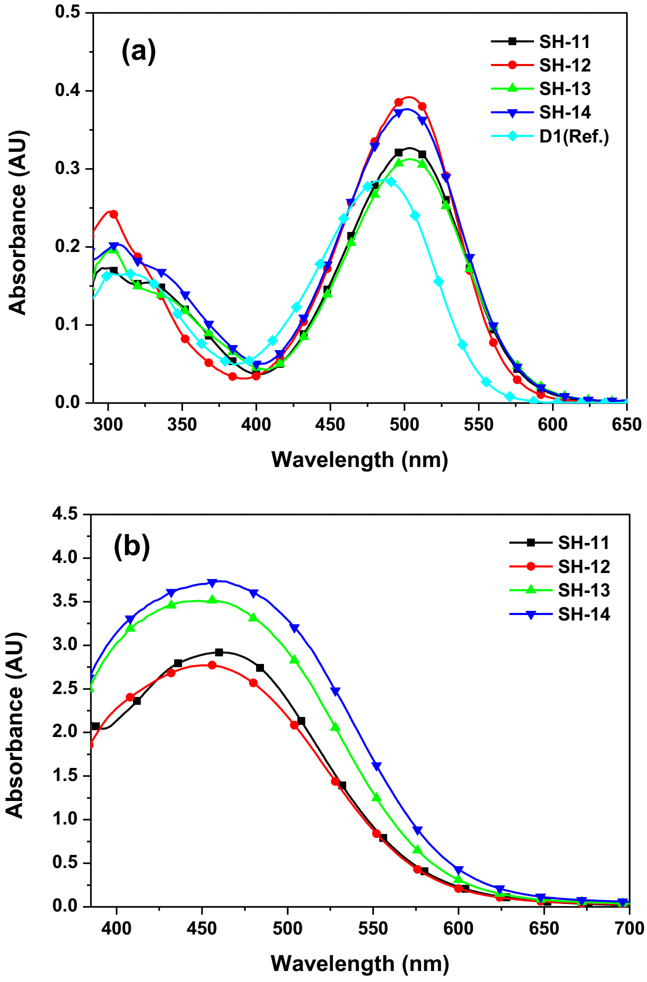

Fig. 2. UV–visible absorption spectra of (a) **D1** and **SH-11~14** in CH_2Cl_2, and (b) **SH-11~14** on TiO_2 films.

ability of the TPA donor, and extended π-electron delocalization over the whole molecule, which red-shifted the absorption maxima by 16–18 nm, compared with that of **D1**. However, the number, position, and shape of methoxy groups attached to the TPA donor had a marginal effect on the maximum absorption of the dyes.

The dye molar extinction coefficients at λ_{max} were also affected by the introduction of additional methoxy groups. In general, the maximum absorption and molar extinction coefficient of dyes are closely related to the transition dipole moment, conjugation length, and planarity [24]. The molar extinction coefficients at λ_{max} of **D1**, **SH-11**, **SH-12**, **SH-13**, and **SH-14** were 28,600, 32,680, 39,200, 31,260, and 37,660 M^{-1} cm^{-1}, respectively. The molar extinction coefficients of **SH-11~14** were all larger than that of **D1**. This could be due to the combined effects of the increased maximum absorption, and the improvement of transition dipole moment by the introduction of additional methoxy groups (Fig. 3). Among the dyes, **SH-12** with methoxy groups at *ortho*- and *para*-position on the TPA donor showed the highest molar extinction coefficient. This could be attributed to the smallest overall dihedral angles (Φ1~3) of the TPA donor part, and that (Φ4) between the TPA donor and the π-bridge, despite the largest dihedral angles of phenyl ring planes (Φ5~6) (Figs. 3 and 4). As for the shape of methoxy groups, the molar extinction coefficient of **SH-14** with closed ring system in the TPA donor part was higher than that of **SH-13** with open ring system. This could be attributed to the improved stereoscopic planarity of the closed ring in the TPA donor, compared to the open ring with protruded methoxy groups. As the number of methoxy groups increased, the molar extinction coefficient generally showed higher figures.

Table 1
Optical and electrochemical properties of **D1** and **SH-11~14**.

Dye	Absorption[a]		Emission[a]	Oxidation potential data[c]		
	λ_{abs}/nm (ε M^{-1} cm^{-1})	λ_{abs}[b]/nm (on TiO_2)	λ_{em}/nm	E_{ox}/V (vs. NHE)	$E_{0\text{-}0}$[d]/V	$E_{ox} - E_{0-0}$/V (vs. NHE)
D1 (Ref.)	486 (28,600)	–	629	0.84	2.25	−1.41
SH-11	504 (32,680)	461	626	0.92	2.15	−1.23
SH-12	504 (39,200)	456	612	0.94	2.19	−1.25
SH-13	504 (31,260)	456	602	0.89	2.15	−1.26
SH-14	502 (37,660)	460	601	0.94	2.16	−1.22

[a] Absorption and emission spectra were measured in CH_2Cl_2 solution at room temperature (1×10^{-5} M).

[b] Absorption spectra on TiO_2 were obtained through measuring the dye absorbed TiO_2 film in CH_2Cl_2.

[c] Oxidation potentials of the dyes were measured in CH_2Cl_2 containing 0.1 M tetrabutylammonium tetrafluoroborate ($TBABF_4$) as electrolyte (working electrode: glassy carbon; counter electrode: Pt; reference electrode: Ag/Ag^+ calibrated with ferrocene/ferrocenium (Fc/Fc^+) as an internal reference, and converted to NHE by the addition of 630 mV [22]).

[d] E_{0-0} was estimated from the onset wavelength of the absorption spectra.

Consequently, the introduction of additional methoxy groups on the TPA donor led to an increase of the electron donating ability of the TPA donor part, and improved the transition dipole moment of the whole molecule. Their introduction also led to the improvement of the whole stereoscopic planarity of the molecule, in comparison with **D1**. Therefore, the absorption maxima and molar extinction coefficients of **SH-11~14** have red-shifted and been enhanced, compared to those of **D1**. This is highly desirable as a photosensitizer for large photocurrent generation. On TiO_2 films, the absorption maxima (λ_{max}) of **SH-11**, **SH-12**, **SH-13**, and **SH-14** are shown in Fig. 2(b). They exhibit large blue-shifts (42–48 nm), due to H-aggregation of the dyes [13,25], or deprotonation of carboxylic acid upon adsorption onto the TiO_2 surface [14b]. Such a hypsochromic shift of the absorption spectra for the dyes has generally been observed in other organic dyes, when dyes are attached to the TiO_2 surface.

3.3. Electrochemical properties of the dyes

The first oxidation potential (E_{ox}), corresponding to each dye's HOMO level, was measured in CH_2Cl_2 by cyclic voltammetry (CV). The excited state oxidation potential ($E_{ox}{}^* = E_{ox} - E_{0-0}$), corresponding to each dye's LUMO level, was obtained by subtracting the zeroth–zeroth energy (E_{0-0}), estimated from the onset wavelength of the absorption spectrum, from E_{ox}. The electrochemical properties of the dyes are listed in Table 1. Their CV curves and HOMO and LUMO level diagram are shown in Figs. 5 and 6, respectively. The HOMO levels of **D1**, **SH-11~14** were 0.84, 0.92, 0.94, 0.89, and 0.94 V, respectively. They were more positive than that of iodine–iodide (0.4 V vs. NHE) [26], and were sufficiently positive to regenerate the oxidized dyes from the redox electrolyte (I^-/I_3^-). As methoxy groups were introduced on the TPA donor part, the HOMO levels of **SH-11~14** became slightly more positive than that of **D1**, which could induce stronger driving force for more efficient dye regeneration. The LUMO levels of **D1**, **SH-11~14** were −1.41, −1.23, −1.25, −1.26, and −1.22 V, respectively. They were sufficiently more negative than the conduction band energy level (E_{cb}) of TiO_2 (−0.5 V vs. NHE) [26], to allow thermodynamically efficient injection of excited electrons into the TiO_2 electrode. The introduction of additional methoxy groups on the TPA donor part made both the HOMO and LUMO levels more positive, in comparison with those of **D1**. The potential increases in LUMO levels were higher than those in HOMO levels, and the energy band gaps (E_{gap}) of the HOMO–LUMO levels were decreased. This may be attributed to increase of the

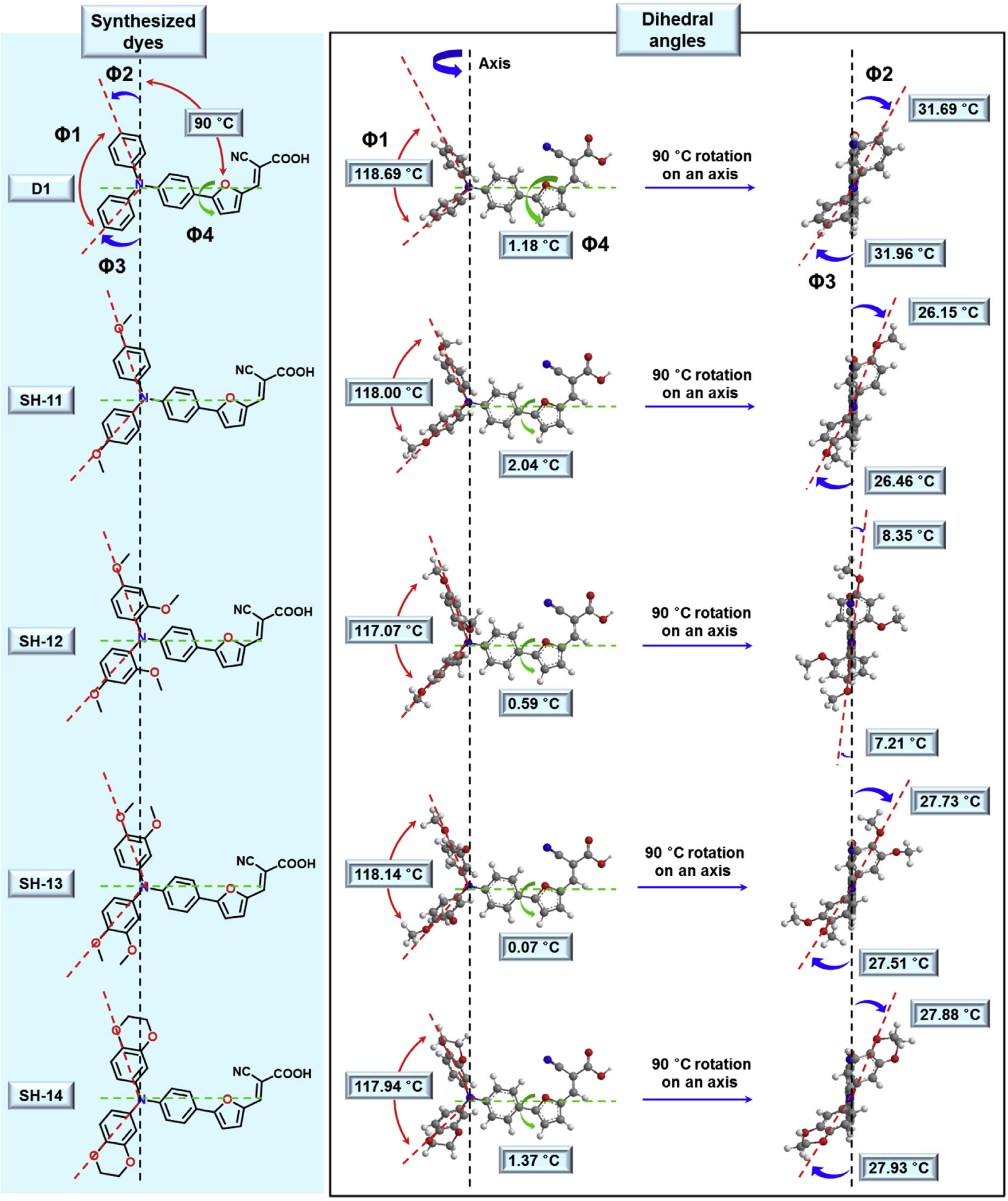

Fig. 3. Dihedral angles of the TPA donor parts (*Φ*1~3), and that between the TPA donor and the π-bridge (*Φ*4) of the synthesized dyes.

electron donating ability of the TPA donor, and the improvement of the stereoscopic planarity of the overall molecule by the change of the dihedral angles (*Φ*1~6) of the dye molecule (Figs. 3 and 4). Consequently, the **SH-11~14** became red-shifted, and might act as more efficient photosensitizers for DSSCs, compared with **D1**.

3.4. Density functional theory (DFT) calculations

To gain further insight into the above results, density functional theory (DFT) calculations of all the dyes were carried out, using the B3LYP/6-31G(d,p) level. The optimized structures, electron distributions, and energy levels of the dyes are presented in Fig. 7. Dihedral angles of the TPA donor parts (*Φ*1~3 and *Φ*5~6), and that between the TPA donor and the π-bridge (*Φ*4) in the dyes, are depicted in Figs. 3 and 4. All the dye electron distributions in the HOMO orbitals were mostly over the TPA donor part and the furan ring. The size of electron distributions of the HOMO orbitals of **SH-11**, **SH-13**, and **SH-14** were larger than that of **D1**. This may be because the electron donating ability of the TPA donor part was improved, by adding methoxy groups as additional electron

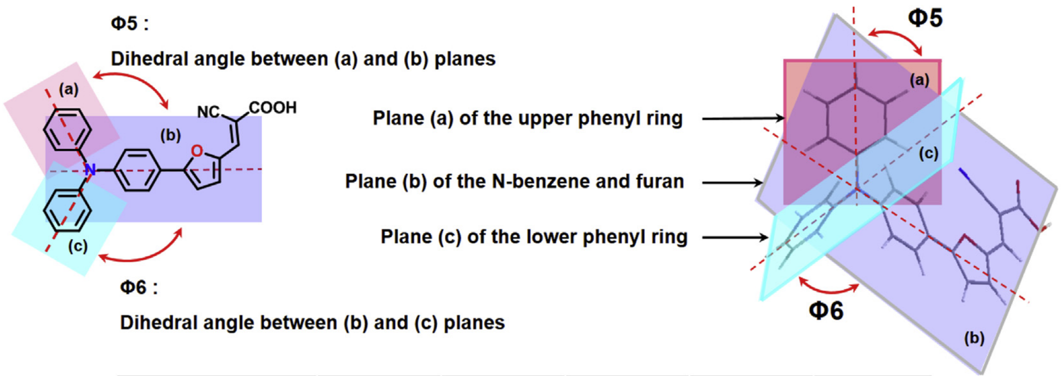

Dihedral angle \ Dye	D1	SH-11	SH-12	SH-13	SH-14
Φ5 (°)	45.8	50.4	74.7	51.2	49.5
Φ6 (°)	46.5	50.0	76.6	48.3	49.8
Average (Φ5~6)	46.15	50.2	75.65	49.75	49.65

Fig. 4. Dihedral angles (*Φ*5~6) between the planes of phenyl rings, and the plane of the *N*-benzene and furan ring.

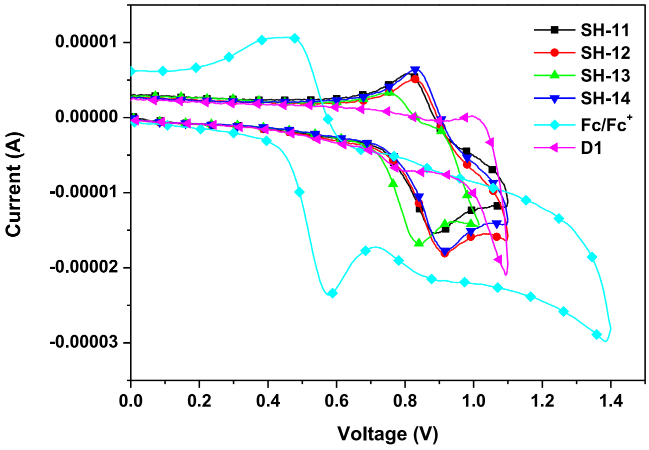

Fig. 5. CV curves of **Fc/Fc**$^+$, **D1**, **SH-11**, **SH-12**, **SH-13**, and **SH-14** in CH_2Cl_2.

donating groups. On the other hand, the size of electron distributions of the HOMO orbitals of **SH-12** was relatively smaller, compared to those of the other dyes. The electron distribution of the HOMO orbital of **SH-12** is mainly over the *N*-benzene ring of the TPA donor connected to the furan ring and the furan ring itself, and seems to be lower over the phenyl rings with methoxy groups, in contrast to the other dyes. This may be due to the largest dihedral angles (*Φ*5~6) between the planes (a, b, c) of phenyl rings, which result in a relatively poor orbital overlap of the TPA donor part. This calculation result can explain why the electrochemical property of **SH-12** is particularly different from those of the other dyes, which will largely affect the cell performance of **SH-12**. All the dye electron distributions of the LUMO orbitals were localized towards the cyanoacrylic acid and its adjacent furan ring. Therefore, the HOMO–LUMO excitation induced by light irradiation could effectively shift the electron distributions from the TPA donor part to the acceptor group. Excited electrons could easily be injected from the dye to the TiO_2 surface by this electron separation. The molecular

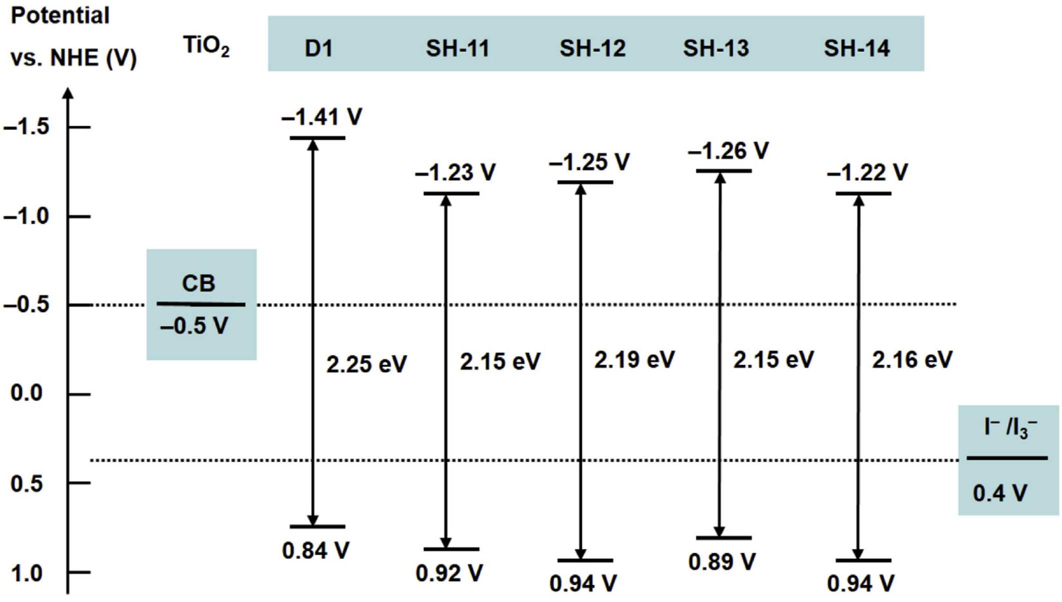

Fig. 6. Dye HOMO and LUMO levels diagram.

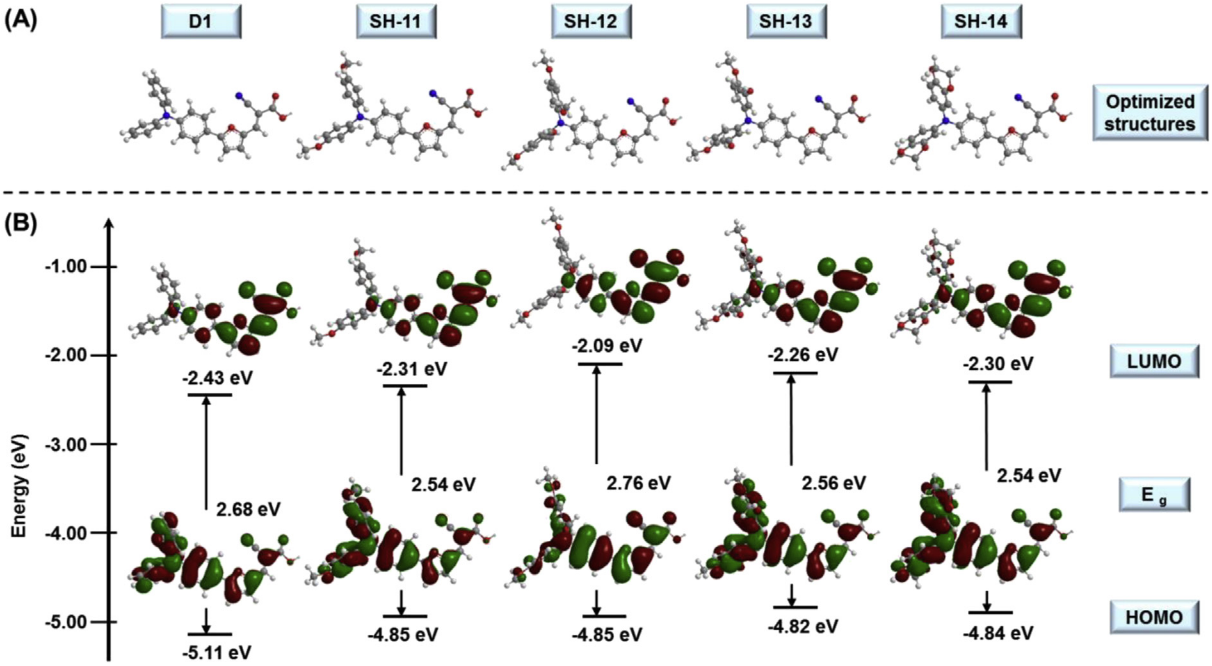

Fig. 7. (A) Plane figures of the dye optimized structures. (B) Dye energy levels and electron distributions through the frontier molecular orbitals of the HOMO and LUMO, calculated with DFT at the B3LYP/6-31G(d,p) level.

structures of **SH-11~14** showed various dihedral angles (*Φ*1~6) as methoxy groups on the introduced TPA donor part. The dihedral angles (*Φ*1) of **SH-11~14** were *ca.* 117–118°, and decreased by *ca.* 1~2°, compared to that of **D1** (*ca.* 119°). The dihedral angles (*Φ*2~3) on an axis of **SH-11~14** were greatly influenced by the introduction of methoxy groups, which decreased by *ca.* 5.5° (**SH-11**), *ca.* 24.0° (**SH-12**), *ca.*4.2° (**SH-13**), and *ca.* 3.9° (**SH-14**), in comparison to that (*ca.* 31.8°) of **D1**. **SH-11**, **SH-13**, and **SH-14** showed similar dihedral angles (*Φ*2~3; *ca.* 26–28°); whereas, **SH-12** showed the largest change of the dihedral angles (*Φ*2~3), due to the steric hindrance induced by methoxy groups at the *ortho*-position adjacent to the *N*-benzene ring. The TPA donor parts of all the dyes had noncoplanar propeller structure that could suppress dye aggregation. The dihedral angles (*Φ*4) of **SH-11~14** were *ca.* 0~2°, and similar to that (*ca.* 1.2°) of **D1**, respectively. This indicates that all the dyes have coplanar structure from the TPA donor part, furan, and to the acceptor group, which can form an efficient conjugation, and hence favor the electron transport process. The dihedral angles (*Φ*5~6) between the planes of phenyl rings and the plane of the *N*-benzene and furan ring have great relevance to the electron density of the TPA donor part, and the inhibition of the close π–π aggregation between dye molecules [17]. The averages of the dihedral angles (*Φ*5~6) of **D1** and **SH-11~14** were 46.15°, 50.2°, 75.65°, 49.75°, and 49.65°, respectively. **SH-11**, **SH-13**, and **SH-14** showed similar dihedral angles (*Φ*5~6; *ca.* 50°); whereas, **SH-12** showed the largest dihedral angles (*Φ*5~6; *ca.* 76°), due to the steric hindrance induced by the methoxy groups at the *ortho*-position adjacent to the *N*-benzene ring. This increase of the dihedral angles (*Φ*5~6) can inhibit close π–π aggregation between the dye molecules, and may decrease the amount of dye adsorbed to the TiO_2 surface. This result explains the amount of dye adsorbed to the TiO_2 surface (Table 2). As a result, the number, position, and shape of methoxy groups introduced on the TPA donor part affected the electron distributions and the dihedral angles (*Φ*1~6) of the dye molecule, which may have contributed to the bathochromic shift of the absorption spectrum, the enhancement of the molar extinction coefficient, and the decrease of the amount of dye adsorbed.

Table 2
Photovoltaic performance data of **D1**, **SH-11**, **SH-12**, **SH-13**, **SH-14**, and **N719**.[a]

Dye[b]	J_{sc}/mA cm^{-2}	V_{oc}/mV	FF/%	η/%	Area (cm^2)	Dye amount[c] (mol cm^{-2})
D1 (Ref.)	10.41	704.3	75.11	5.51	0.269	2.73×10^{-7}
SH-11	11.96	691.6	67.37	5.57	0.275	2.16×10^{-7}
SH-12	9.89	578.5	67.29	3.85	0.274	1.43×10^{-7}
SH-13	11.39	676.3	68.66	5.29	0.275	2.31×10^{-7}
SH-14	12.29	687.5	71.18	6.01	0.284	2.35×10^{-7}
N719	13.60	783.3	71.26	7.59	0.279	–

[a] Measured under AM 1.5 irradiation G (100 mW cm^{-1}), with 0.269–0.284 cm^2 working area.

[b] Dyes were maintained at 0.5 mM in *tert*-butanol–acetonitrile (1:1) solution, with 10 mM CDCA as co-adsorbent. Electrolyte comprised 0.7 M 1-methyl-3-propylimidazolium iodide (MPII), 0.2 M LiI, 0.05 M I_2, 0.5 M TBP in acetonitrile–valeronitrile (v/v, 85/15) for organic dyes.

[c] The amount of dyes adsorbed on TiO_2 was measured by a colorimetric method, using 0.1 M NaOH aqueous-DMF (1:1) mixed solutions to wash the dyes off the TiO_2 film.

3.5. *Photovoltaic properties of DSSCs*

DSSCs were fabricated using the dyes as photosensitizers, and their photovoltaic properties were measured under AM 1.5G irradiation (100 mW cm^{-2}). The effects on cell performance by the number, position, and shape of methoxy groups attached to the TPA moiety were assessed, by measuring their conversion efficiencies, relative to the **D1** as a reference. The capabilities of all the dyes as possible photosensitizers were compared with **N719** cell performance (Table 2). Fig. 8(a) and (b) shows the incident photon-to-current conversion efficiency (IPCE) spectra and photocurrent–voltage (*J*–*V*) curves, respectively. All the dyes could effectively convert visible light to photocurrent at *ca.* 300–700 nm. The IPCE value of the cell with **D1** as a reference exceeded 80% from 400 to 540 nm, with the highest value of 86.3% at 490 nm. The IPCE value of the cells with **SH-11** exceeded 80% from 430 to 550 nm, with the highest value of 84.2% at 500 nm. The IPCE values of the cells with **SH-13** (open ring system) and **SH-14** (closed ring system) exceeded 80% from 480 to 500 nm and from 430 to 540 nm, with the highest values of 80.6% and 83.4% at 490 nm, respectively. In contrast with the above dyes, the IPCE value of the cells with **SH-12** did not show over 80% in the range, and the highest value was 79.0% at 490 nm. Contrary to expectations, **SH-12** with the highest molar extinction coefficient and λ_{max} showed the lowest IPCE value among them, which may be due to a poor orbital overlap by the largest dihedral angles (Φ5~6) [11b]. Although the IPCE value of the cell with **N719** as the other reference also did not show over 80% in the range, its IPCE spectrum had the broadest region, and the highest value was 76.1% at 500 nm. Except for **SH-12**, other dyes (**SH-11** and **SH-13~14**) can convert visible light to photocurrent more efficiently than **D1** at the whole wavelength range (*ca.* 300–700 nm). These results can be closely linked to the J_{sc} values of the dyes.

The J_{sc} values of all the dye cells ranked **SH-12** < **D1** < **SH-13** < **SH-11** < **SH-14** (**SH-12**, 9.89; **D1**, 10.41; **SH-13**, 11.39; **SH-11**, 11.96; **SH-14**, 12.29 mA cm^{-2}), and are similar to the result of IPCE values. Except for **SH-12**, the J_{sc} values of the other dyes (**SH-11** and **SH-13~14**) showed higher J_{sc} values than that of **D1**. Though the dihedral angles (Φ5~6) of **SH-11** and **SH-13~14** increased a little by the introduction of additional methoxy groups at the TPA donor part, their introduction led to bathochromic shift and enhancement of the molar extinction coefficient by the increase of electron donating ability, improving the J_{sc} values. However, **SH-12** resulted in the lowest J_{sc} value, due to the largest dihedral angles (Φ5~6), which decreased the electron density of the TPA donor part, by forming a relatively poor orbital overlap between the two planes. The J_{sc} value was also likely to be affected by the amount of dye adsorbed to the TiO_2 surface, which was influenced by the steric hindrance induced by the introduction of methoxy groups on the TPA donor part (Table 2).

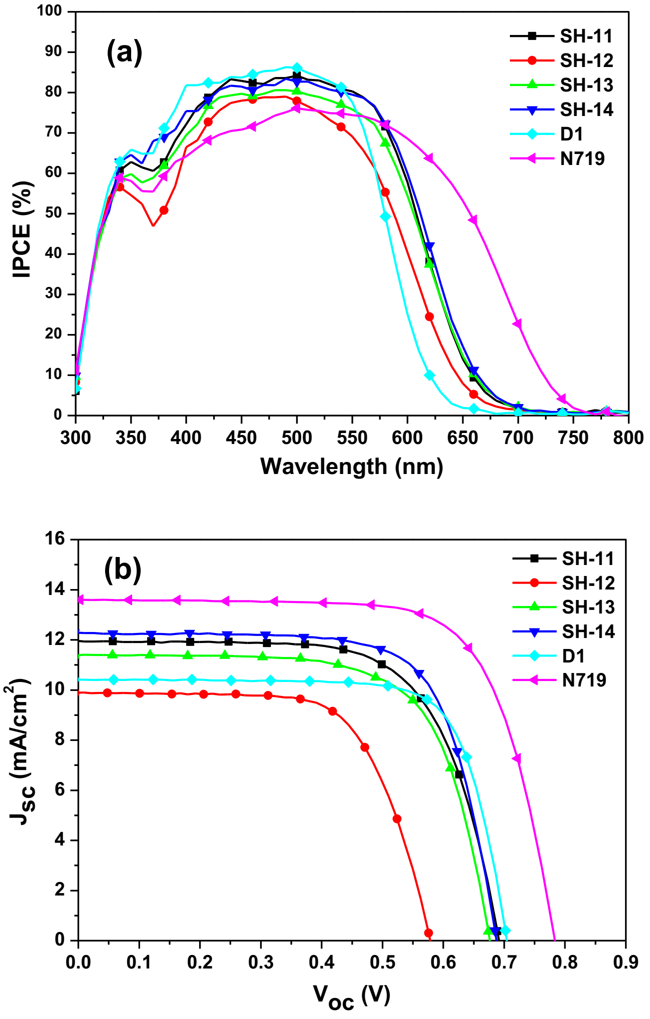

Fig. 8. (a) Incident photo-to-current conversion efficiency (IPCE) spectra for DSSCs based on **SH-11**, **SH-12**, **SH-13**, **SH-14**, **D1**, and **N719**. (b) Photocurrent–voltage curves for DSSCs based on **SH-11**, **SH-12**, **SH-13**, **SH-14**, **D1**, and **N719**, under illumination of AM 1.5G simulated sunlight (100 mW cm^{-2}).

The amount of dye adsorbed increased in the order of **SH-12** ≪ **SH-11** ≤ **SH-13** ≈ **SH-14** < **D1** (**SH-12**, 1.43 × 10^{-7}; **SH-11**, 2.16 × 10^{-7}; **SH-13**, 2.31 × 10^{-7}; **SH-14**, 2.35 × 10^{-7}; **D1**, 2.73 × 10^{-7} mol cm^{-2}). This order coincides with the tendency of decreasing steric hindrance by dihedral angles (Φ5~6), which signify the twisted degree of the phenyl rings on the backbone plane (b) of dyes (Fig. 4). This indicates that the increase of steric hindrance could decrease the amount of dye adsorbed to the TiO_2 surface, by suppressing close π–π aggregation between the dye molecules. As a result, all things considered, **SH-14** with a high molar extinction coefficient, small dihedral angles (Φ5~6), and a relatively high amount of dye adsorbed, showed the largest J_{sc} value. Though **SH-12** had a high molar extinction coefficient and red-shifted, the dye showed the lowest J_{sc} value, due to the least amount of dye adsorbed, and relatively poor orbital overlap by the largest dihedral angles (Φ5~6) of the TPA donor part.

The V_{oc} values ranked **SH-12** (578.5 mV) ≪ **SH-13** (676.3 mV) < **SH-14** (687.5 mV) ≤ **SH-11** (691.6 mV) < **D1** (704.3 mV). The V_{oc} values of all the dyes decreased, as the number of methoxy groups increased. This may be due to the decease of the amount of dye adsorbed, and the formation of iodine-electron donor complexes. The decease of the amount of dye adsorbed was mainly attributed to the lower packing density of dyes on the TiO_2 surface, which could result in higher I_3^- concentration in the vicinity of the TiO_2 surface, and increase the possibility of electron recombination, compared to **D1** [17]. In addition, it has been reported that iodine has the tendency to form iodine-electron donor complexes with atoms that contain lone-pair electrons, such as oxygen, nitrogen, and sulfur [11b]. Therefore, **SH-11~14** is more likely than **D1** to form dye–iodine complexes, due to the presence of the additional methoxy groups. Accordingly, the presence of the additional methoxy groups could naturally increase I_3^- concentration near the TiO_2 surface. Consequently, as the number of methoxy groups increases, more dye–iodine complexes will form, and subsequently result in enhanced electron recombination, in comparison to **D1**. **D1** without methoxy groups showed the highest V_{oc} value; and **SH-11** with two methoxy groups at *para*-position also showed a higher V_{oc} value than **SH-12~14** with four methoxy groups. Dyes with four methoxy groups showed different V_{oc} values, depending on the position and shape of the methoxy groups. The V_{oc} value of **SH-12** was far lower than those of **SH-13~14**, which is mainly attributed to the decease of the amount of dye adsorbed, and the improvement of I_3^- accessibility by the increase of dihedral angles (Φ5~6) induced by the steric hindrance of methoxy groups at *ortho*-position adjacent to the *N*-benzene ring.

In shape, **SH-14** with a closed ring system of methoxy groups had slightly higher V_{oc} value, compared with **SH-13** with an open ring system of methoxy groups. This means that methoxy groups in the closed ring blocked the approach of I_3^- more effectively, compared to methoxy groups in the open ring. Although the amount of **SH-11** adsorbed was relatively lower than those of **SH-13~14**, the V_{oc} value of **SH-11** was a bit higher than those of **SH-13~14**, which might be because the number of methoxy groups has a greater impact on V_{oc} value, compared with the amount of dye adsorbed. FF values slightly decreased on introducing methoxy groups on the TPA donor part. The decreased order coincides with the increased order of dihedral angles (Φ5~6). These results indicate that FF values could be affected by the shape of photosensitizer.

D1, **SH-11**, **SH-12**, **SH-13**, **SH-14**, and **N719** dyes' η values were 5.51%, 5.57%, 3.85%, 5.29%, 6.01%, and 7.59%, respectively, under AM 1.5G irradiation (100 mW cm^{-2}) (Table 2). Through the introduction of methoxy groups on the TPA donor part, η values of **SH-11** and **SH-14** improved, due to the larger increase of J_{sc} values than the decrease of V_{oc} and FF values, compared to **D1**. Although **SH-13** showed the higher J_{sc} value than **D1**, **SH-13** dye η value was less, due to the larger decrease of V_{oc} and FF value. **SH-12** showed the lowest η value, because of its small adsorption on the TiO_2 surface, and relatively poor orbital overlap by the largest dihedral angles (Φ5~6). Consequently, all things considered, the best overall conversion efficiency was achieved by the cell fabricated with **SH-14** ($\eta = 6.01\%$, $J_{sc} = 12.29$ mA/cm^2, $V_{oc} = 687.5$ mV, FF = 71.18% under AM 1.5G irradiation), reaching about 79.2% of **N719** dye's 7.59%.

3.6. *Electrochemical impedance spectroscopy (EIS)*

Electrochemical impedance spectroscopy (EIS) analysis [27] was employed to investigate the electron recombination and interfacial charge transfer process in DSSCs. The EIS spectra for the DSSCs based on **SH-11~SH-14** were performed under forward bias (−0.65 V) in the dark. The Nyquist and Bode phase plots of DSSCs are shown in Fig. 9(a) and (b), respectively. The major semicircles and frequency peaks in the Nyquist and Bode phase plots indicate the charge transfer resistance at the TiO_2/dye/electrolyte interface. The radii of the major semicircles in the Nyquist plots increase in the order of **SH-12** < **SH-13** < **SH-14** < **SH-11**, indicating that the electron recombination resistance increases from **SH-12**, **SH-13**, **SH-14** to **SH-11**. The major frequency peaks in the Bode phase plots lower in the order of **SH-12** > **SH-13** > **SH-14** > **SH-11**, indicating that the electron lifetime increases in the order of **SH-12** < **SH-13** < **SH-14** < **SH-11**. A larger electron recombination resistance and longer electron lifetime indicate improved suppression of back reactions between the injected electrons (e^-) and the electrolyte (I_3^-); they lead to improvement of the V_{oc} value, due to the reduced electron recombination rate [28]. The ranking of the cell electron recombination resistances and electron lifetimes measured by EIS coincided with that of the cell V_{oc} values. Consequently, these results indicate that as the number of methoxy groups and dihedral angles (Φ1~6) of a dye increase, the electron recombination resistance decreases and electron lifetime shortens, due to the improvement of accessibility between the injected electrons (e^-) and the electrolyte (I_3^-).

4. Conclusion

New triphenylamine-based organic dyes with AD–D–π–A structure (**SH-11~14**) were designed and synthesized, to study the effects of the number, position, and shape of methoxy groups attached to the TPA donor on the dye photophysical and electrochemical properties and the cell photovoltaic performance in DSSCs.

The introduction of methoxy groups as an additional donor on the TPA donor led to bathochromic shift of the absorption spectrum and enhancement of the molar extinction coefficient of the dyes, due to increase of the electron donating ability of the TPA donor part, and the extension of π-electron delocalization over the whole molecule. Their introduction also led to decrease of the amount of dye adsorbed, due to the increased steric hindrance afforded by protruding methoxy groups toward the backbone plane (b) of the molecule.

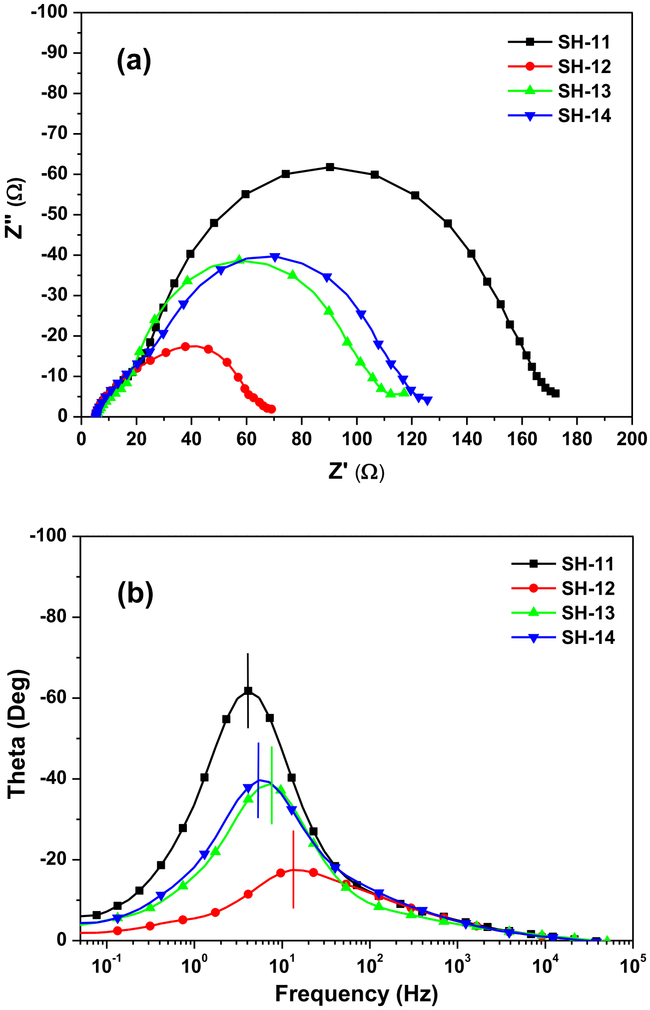

Fig. 9. EIS spectra of DSSCs based on **SH-11**, **SH-12**, **SH-13**, and **SH-14** measured at −0.65 V forward bias in the dark: (a) Nyquist, and (b) Bode phase plots.

The J_{sc} values of other dyes (**SH-11** and **SH-13~14**) except **SH-12** generally increased, as the methoxy groups were introduced. Among the organic dyes, **SH-14** with a high molar extinction coefficient, small dihedral angles (Φ5~6), and a relatively high amount of dye adsorbed, showed the highest J_{sc} value.

The V_{oc} values of all the dyes decreased, as the number of methoxy groups increased. This may be due to decease of the amount of dye adsorbed by the increase of overall steric hindrance and the formation of iodine-electron donor complexes by the lone-pair electrons in the methoxy groups.

As a result, the highest solar energy-to-electricity conversion efficiency was achieved with **SH-14**, which had the maximum η value of 6.01% ($J_{sc} = 12.29$ mA/cm^2, $V_{oc} = 687.5$ mV, FF = 71.18%) under AM 1.5G irradiation. These results indicate that dye J_{sc}, V_{oc}, and η values are greatly influenced by the number, position, and shape of additional methoxy groups attached to the TPA donor, and that novel TPA donor of closed ring shape, such as **SH-14**, can be promising electron donor for higher performance of DSSCs. We will be able to achieve better performance, by introducing appropriate π-bridges (–A–π–) that improve stereoscopic planarity in AD–D–A–π–A structure.

References

[1] O'Regan B, Grätzel M. A low-cost, high-efficiency solar cell based on dye-sensitized colloidal TiO_2 films. Nature 1991;353:737–40.

[2] (a) Qin Y, Peng Q. Ruthenium sensitizers and their applications in dye-sensitized solar cells. Int J Photoenergy 2012:1–21;
(b) Zhang S, Yang X, Numata Y, Han L. Highly efficient dye-sensitized solar cells: progress and future challenges. Energy Environ Sci 2013;6:1443–64;
(c) Li L-L, Diau EW-G. Porphyrin-sensitized solar cells. Chem Soc Rev 2013;42:291–304;
(d) Liang M, Chen J. Arylamine organic dyes for dye-sensitized solar cells. Chem Soc Rev 2013;42:3453–88.

[3] (a) Grätzel M. Dye-sensitized solar cells. J Photochem Photobiol C 2003;4:145–53;
(b) Grätzel M. Conversion of sunlight to electric power by nanocrystalline dye-sensitized solar cells. J Photochem Photobiol A Chem 2004;164(3):3–14;
(c) Park N-G, Kim K. Transparent solar cells based on dye-sensitized nanocrystalline semiconductors. Phys Status Solidi A 2008;205(8):1895–904;
(d) Zeng WD, Cao Y, Bai Y, Wang Y, Shi Y, Zhang M, et al. Efficient dye-sensitized solar cells with an organic photosensitizer featuring orderly conjugated ethylenedioxythiophene and dithienosilole blocks. Chem Mater 2010;22:1915–25;
(e) Yang J, Ganesan P, Teuscher J, Moehl T, Kim YJ, Yi C, et al. Influence of the donor size in D–π–A organic dyes for dye-sensitized solar cells. J Am Chem Soc 2014;136:5722–30.

[4] Yella A, Lee H-W, Tsao HN, Yi C, Chandiran AK, Nazeeruddin MdK, et al. Porphyrin-sensitized solar cells with cobalt (II/III)-based redox electrolyte exceed 12 percent efficiency. Science 2011;334:629–34.

[5] (a) Koumura N, Wang Z-S, Miyashita M, Uemura Y, Sekiguchi H, Cui Y, et al. Substituted carbazole dyes for efficient molecular photovoltaics: long electron lifetime and high open circuit voltage performance. J Mater Chem 2009;19:4829–36;
(b) Sudyoadsuk T, Pansay S, Morada S, Rattanawan R, Namuangruk S, Kaewin T, et al. Synthesis and characterization of D–D–π–A-type organic dyes bearing carbazole–carbazole as a donor moiety (D–D) for efficient dye-sensitized solar cells. Eur J Org Chem 2013;23:5051–63;
(c) Cai S, Tian G, Li X, Su J, Tian H. Efficient and stable DSSC sensitizers based on substituted dihydroindolo[2,3-b]carbazole donors with high molar extinction coefficients. J Mater Chem A 2013;1:11295–305.

[6] (a) Wang Z-S, Cui Y, Dan-oh Y, Kasada C, Shinpo A, Hara K. Thiophene-functionalized coumarin dye for efficient dye-sensitized solar cells: electron lifetime improved by coadsorption of deoxycholic acid. J Phys Chem C 2007;111(19):7224–30;
(b) Wang Z-S, Cui Y, Hara K, Dan-oh Y, Kasada C, Shinpo A. A high-light-harvesting-efficiency coumarin dye for stable dye-sensitized solar cells. Adv Mater 2007;19(8):1138–41.

[7] Kim S, Lee JK, Kang SO, Ko J, Yum J-H, Fantacci S, et al. Molecular engineering of organic sensitizers for solar cell applications. J Am Chem Soc 2006;128(51):16701–7.

[8] Ito S, Miura H, Uchida S, Takata M, Sumioka K, Liska P. High-conversion efficiency organic dye-sensitized solar cells with a novel indoline dye. Chem Commun 2008;41:5194–6.

[9] Li C, Yum J-H, Moon S-J, Herrmann A, Eickemeyer F, Pschirer NG, et al. An improved perylene sensitizer for solar cell applications. ChemSusChem 2008;1(7):615–8.

[10] (a) Kim SH, Kim HW, Sakong C, Namgoong J, Park SW, Ko MJ, et al. Effect of five-membered heteroaromatic linkers to the performance of phenothiazine-based dye-sensitized solar cells. Org Lett 2011;13:5784–7;
(b) Kim SH, Sakong C, Chang JB, Kim B, Ko MJ, Kim DH, et al. The effect of N-substitution and ethylthio substitution on the performance of phenothiazine donors in dye-sensitized solar cells. Dyes Pigments 2013;97:262–71;
(c) Hua Y, Chang S, Huang D, Zhou X, Zhu X, Zhao J, et al. Significant improvement of dye-sensitized solar cell performance using simple phenothiazine-based dyes. Chem Mater 2013;25:2146–53.

[11] (a) Tian H, Bora I, Jiang X, Gabrielsson E, Karlsson KM, Hagfeldt A, et al. Modifying organic phenoxazine dyes for efficient dye-sensitized solar cells. J Mater Chem 2011;21:12462–72;
(b) Karlsson KM, Jiang X, Eriksson SK, Gabrielsson E, Rensmo H, Hagfeldt A, et al. Phenoxazine dyes for dye-sensitized solar cells: relationship between molecular structure and electron lifetime. Chem Eur J 2011;17:6415–24.

[12] Qin C, Wong W-Y, Han L. Squaraine dyes for dye-sensitized solar cells: recent advances and future challenges. Chem Asian J 2013;8:1706–19.

[13] Chen R, Yang X, Tian H, Sun L. Tetrahydroquinoline dyes with different spacers for organic dye-sensitized solar cells. J Photochem Photobiol A Chem 2007;189:295–300.

[14] (a) Liu W-H, Wu I-C, Lai C-H, Lai C-H, Chou P-T, Li Y-T, et al. Simple organic molecules bearing a 3,4-ethylenedioxythiophene linker for efficient dye-sensitized solar cells. Chem Commun 2008;41:5152–4;
(b) Lin L-Y, Tsai C-H, Wong K-T, Huang T-W, Hsieh L, Liu S-H, et al. Organic dyes containing coplanar diphenyl-substituted dithienosilole core for efficient dye-sensitized solar cells. J Org Chem 2010;75:4778–85;
(c) Liang Y, Peng B, Liang J, Tao Z, Chen J. Triphenylamine-based dyes bearing functionalized 3,4-propylenedioxythiophene linkers with enhanced performance for dye-sensitized solar cells. Org Lett 2010;12:1204–7;
(d) Jiang X, Karlsson KM, Gabrielsson E, Johansson EMJ, Quintana M, Karlsson M, et al. Highly efficient solid-state dye-sensitized solar cells based on triphenylamine dyes. Adv Funct Mater 2011;21:2944–52;
(e) Sakong C, Kim SH, Yuk SB, Namgoong JW, Park SW, Ko MJ, et al. Influence of solvent and bridge structure in alkylthio-substituted triphenylamine dyes on the photovoltaic properties of dye-sensitized solar cells. Chem Asian J 2012;7:1817–26;
(f) Tian H, Yang X, Chen R, Zhang R, Hagfeldt A, Sun L. Effect of different dye baths and dye-structures on the performance of dye-sensitized solar cells based on triphenylamine dyes. J Phys Chem C 2008;112:11023–33;
(g) Ning Z, Tian H. Triarylamine: a promising core unit for efficient photovoltaic materials. Chem Commun 2009:5483–95.

[15] Hagfeldt A, Boschloo G, Sun L, Kloo L, Pettersson H. Dye-sensitized solar cells. Chem Soc Rev 2010;110:6595–663.

[16] (a) Gather MC, Bradley DDC. An improved optical method for determining the order parameter in thin oriented molecular films and demonstration of a highly axial dipole moment for the lowest energy p–p* optical transition in poly(9,9-dioctylfluorene-co-bithiophene). Adv Funct Mater 2007;17:479–85;
(b) Fink RF, Seibt J, Engel V, Renz M, Kaupp M, Lochbrunner S, et al. Exciton trapping in π-conjugated materials: a quantum-chemistry-based protocol applied to perylene bisimide dye aggregates. J Am Chem Soc 2008;130:12858–9.

[17] Tan L-L, Chen H-Y, Hao L-F, Shen Y, Xiao L-M, Liu J-M, et al. Starburst triarylamine based dyes bearing a 3,4-ethylenedioxythiophene linker for efficient dye-sensitized solar cells. Phys Chem Chem Phys 2013;15:11909–17.

[18] (a) Ning Z, Zhang Q, Wu W, Pei H, Liu B, Tian H. Starburst triarylamine based dyes for efficient dye-sensitized solar cells. J Org Chem 2008;73:3791–7;
(b) Hagberg DP, Jiang X, Gabrielsson E, Linder M, Marinado T, Brinck T, et al. Symmetric and unsymmetric donor functionalization. comparing structural and spectral benefits of chromophores for dye-sensitized solar cells. J Mater Chem 2009;19:7232–8;
(c) Zhang M-D, Pan H, Ju X-H, Ji Y-J, Qin L, Zheng H-G, et al. Improvement of dye-sensitized solar cells' performance through introducing suitable heterocyclic groups to triarylamine dyes. Phys Chem Chem Phys 2012;14:2809–15;
(d) Bonnier C, Machin DD, Abdi OK, Robson KCD, Koivisto BD. The effect of donor-modification in organic light-harvesting motifs: triphenylamine donors appended with polymerisable thienyl subunits. Org Biomol Chem 2013;11:7011–5.

[19] Lin JT, Chen P-C, Yen Y-S, Hsu Y-C, Chou H-H, Yeh M-CP. Organic dyes containing furan moiety for high-performance dye-sensitized solar cells. Org Lett 2009;11:97–100.

[20] Park SW, Son K-I, Ko MJ, Kim K, Park N-G. Effect of donor moiety in organic sensitizer on spectral response, electrochemical and photovoltaic properties. Synth Met 2009;159:2571–7.

[21] Santos PF, Reis LV, Duarte I, Serrano JP, Almeida P, Oliveira AS, et al. Synthesis and photochemical evaluation of iodinated squarylium cyanine dyes. Helv Chim Acta 2005;88:1135–43.

[22] Hagberg DP, Edvinsson T, Marinado T, Boschloo G, Hagfeldt A, Sun L. A novel organic chromophore for dye-sensitized nanostructured solar cells. Chem Commun 2006:2245–7.

[23] Thomas KRJ, Hsu Y-C, Lin JT, Lee K-M, Ho K-C, Lai C-H, et al. 2,3-Disubstituted thiophene-based organic dyes for solar cells. Chem Mater 2008;20:1830–40.

[24] (a) In: Gordon PF, Gregory P, editors. Organic chemistry in colour. Berlin Heidelberg: Springer-Verlag; 1987. p. 23–261;
(b) Tsai M-S, Hsu Y-C, Lin JT, Chen H-C, Hsu C-P. Organic dyes containing 1H-phenanthro[9,10-d]imidazole conjugation for solar cells. J Phys Chem C 2007;111:18785–93.

[25] (a) Tian H, Yang X, Chen X, Pan Y, Li L, Hagfeldt A, et al. Phenothiazine derivatives for efficient organic dye-sensitized solar cells. Chem Commun 2007:3741–3;
(b) Hara K, Wang Z-S, Sato T, Furube A, Katoh R, Sugihara H, et al. Oligothiophene-containing coumarin dyes for efficient dye-sensitized solar cells. J Phys Chem B 2005;109:15476–82.

[26] Hagfelt A, Grätzel M. Light-induced redox reactions in nanocrystalline systems. Chem Rev 1995;95:49–68.

[27] (a) Bisquert J. Chemical capacitance of nanostructured semiconductors: its origin and significance for nanocomposite solar cells. Phys Chem Chem Phys 2003;5:5360–4;
(b) Wang Q, Moser J-E, Grätzel M. Electrochemical impedance spectroscopic analysis of dye-sensitized solar cells. J Phys Chem B 2005;109:14945–53.

[28] Kuang D, Uchida S, Humphry-Baker R, Zakeeruddin SM, Grätzel M. Organic dye-sensitized ionic liquid based solar cells: remarkable enhancement in performance through molecular design of indoline sensitizers. Angew Chem Int Ed 2008;47:1923–7.